Individual tree species classification from airborne multi-sensor imagery

Juheon Lee[a,b], Xiaohao Cai[a,b], Jan Lellmann[b], Michele Dalponte[a,c], Yadvinder Malhi[d], Nathalie Butt[d,e], Mike Morecroft[f], Carola-Bibiane Schönlieb[b], and David A. Coomes[a]

[a]Forest Ecology and Conservation Group, Department of Plant Sciences, University of Cambridge, CB2 3EA, UK

[b]Image Analysis Group, Department of Applied Mathematics and Theoretical Physics (DAMTP), University of Cambridge, CB3 0WA, UK

[c] Department of Sustainable Agro-ecosystems and Bioresources, Research and Innovation Centre, Fondazione E. Mach, Via E. Mach 1, 38010 San Michele all'Adige (TN), Italy

[d] Environmental Change Institute, School of Geography and the Environment, University of Oxford, OX1 3QY, UK

[e] Centre for Biodiversity and Conservation Science, The University of Queensland, St Lucia, 4072, Qld, Australia

[f] Natural England, Cromwell House, 15 Andover Road, Winchester, SO23 7BT, UK

Abstract

Remote sensing of individual tree species has many applications in resource management, biodiversity assessment and conservation. Airborne remote sensing using LiDAR and hyperspectral sensors has been used extensively to extract biophysical traits of vegetation and to detect species. However, its application for individual tree mapping remains limited due to the technical challenges of precise co-alignment of images acquired from different sensors and accurately delineating individual tree crowns (ITCs). In this study we developed a generic workflow to map tree species at ITC-level from hyperspectral imagery and LiDAR data using a combination of well-established and recently developed techniques. The workflow uses a non-parametric image registration approach to co-align images, a multi-class normalised graph cut method for ITC delineation, robust principal component analysis for feature extraction, and support vector machine for species classification. This workflow allows us to automatically map tree species at both pixel- and ITC-level. Experimental tests of the technique were conducted using ground data collected from a fully-mapped temperate woodland in the UK. The overall accuracy of pixel-level classification was 89%, while that of ITC-level classification was 66%. The test results demonstrate the effectiveness of the approach.

Index Terms

Hyperspectral imaging, LiDAR, image registration, image segmentation, species classification, PCA, SVM, Wytham Woods

I. Introduction

Having maps of individual tree locations is fundamental to understanding forest responses to global change, providing a basis for monitoring species distribution patterns, responses to stress, disease and exotic-species spread and deforestation [1]. Mapping species using conventional surveying methods require a large amount of time and effort so few tree maps extend beyond 50-ha (50 hectares) in extent; larger scale maps have been generated by sampling in small plots distributed over wider regions and interpolating [2]. The development of sophisticated remote sensing technologies is making it increasingly feasible to monitor single trees in forests using satellites or aircraft. Satellite based multi-spectral sensors, such as WorldView-2, provide high resolution imagery covering visible and near infrared channels. These sensors are increasingly used for mapping species, but their effectiveness in species discrimination varies from study to study due to limited spectral resolution [3]–[6]. Airborne hyperspectral sensors, on the other hand, can measure spectral properties of a target in narrow bands spread from visible to short-wave infrared wavelengths of the electromagnetic spectrum (400–2500nm). Studies carried on with handheld hyper-spectrometers show that species are often distinguishable from their leaf reflectance spectra, even in diverse tropical forests [7], [8]. For example, about half of 188 species sampled from a humid tropical forest in Hawaii could be distinguished from their spectra, with differential reflectance in the SWIR as well as the visible and NIR being important [8], [9]. Such results prognosticate the identification of individual trees by remote sensing with similar sensors [10]–[13].

Airborne hyperspectral imaging provides spectral properties of the vegetation canopies, which can be used to identify tree species. Scaling-up species classification from leaf level to canopy level remains challenging as reflectance signals of mixed vegetation canopy are influenced by leaf density, leaf angle distribution, crown shape and shading [12]. Nevertheless, recent studies have successfully used hyperspectral imaging to map species in tropical forests [9], [14], [15], savanna woodlands [16], [17], Mediterranean woodlands [18], [19], temperate deciduous forests [20], [21] and boreal forests [22]. Clark *et al.* [14] pioneered the use of hyperspectral data to identify canopy species in tropical rain forest, detecting seven tree species with 92% accuracy. Cho *et al.* [23] detected ten tree species with 57% accuracy in the lowveld woodlands of South Africa. Dalponte *et al.* [18] classified 23 species from two Mediterranean woodlands, and achieved 88% and 96% accuracy for those regions. Therefore, rapid advances are being made in this context.

The accuracy of pixel-level species maps can be improved by combining features from Light Detection And Ranging (LiDAR) and hyperspectral imagery in classification algorithms. LiDAR produces 3D point clouds indicating tree positions, from which canopy height and various other metrics can be extracted for each pixel. Features comprised of this structural information complement the optical data provided by hyperspectral sensors, particularly as LiDAR data is not influenced by illumination artifacts such as shading of shorter trees by their taller neighbours [24]. High species classification accuracy (89%) in an Italian temperate floodplain forest was achieved fusing LiDAR and hyperspectral imagery before classification [24]. Jones *et al.* [25] showed that LiDAR and hyperspectral fusion can improve species classification in a mixed broadleaf-conifer forest. The work in [26] also showed that improvement was observed when LiDAR and hyperspectral imagery were used together in alpine forests containing a mixture of beech and conifers. However, the importance of LiDAR-derived features on classification success varies greatly among species [25]–[27].

The approaches described above illustrate the advances made in pixel-based classification, but less progress has been made

in mapping individual tree crowns (ITCs) using multi-sensor techniques. The 3D point clouds provided by LiDAR provide an excellent data for ITC delineation [24]–[28], while canopy spectral information can be obtained from the corresponding pixels of hyperspectral imagery within each of the identified crowns, so in principle this combination of information is powerful [23], [29]–[33]. Mapping species at single tree scale has been demonstrated in urban environments, where trees are sparsely distributed [30]–[32]. For example, Alonzo *et al.* [32] mapped 30 urban tree species at ITC-level using full spectral bands of hyperspectral imagery and seven tree structural parameters derived from LiDAR. However, for more complex environments, we know of only three studies that have investigated ITC-level species classification using a multi-sensor approach: Colgan *et al.* delineated ITCs from LiDAR and classified species from hyperspectral imagery in a savanna woodland, then combined these results [23]. Dinuls *et al.* [34] extracted tree tops from LiDAR, then classify five species from corresponding pixels taken from multi-spectral imagery. Heinzel and Koch showed that under-segmentation of ITCs using LiDAR-based delineation could be rectified by using species classification information alongside LiDAR [29]. Dalponte *et al.* improved species classification by selecting pixels inside of ITCs for training species for the classification and excluding all others [33].

This paper develops a generic workflow for tree species classification at ITC-level from LiDAR and hyperspectral sensors. We deal with several technical challenges:

- Multi-sensor imaging requires images recorded by various sensors to be co-aligned, but different sensor characteristics result in scale, rotation or translation mismatches between images, making correction a pre-requisite. Our workflow includes a image registration step using the NGF-Curv method [35] to co-align hyperspectral imagery and LiDAR.
- Locating ITCs in the 3D LiDAR point cloud or optical imagery requires an accurate tree delineation algorithm, but most established approaches are inaccurate in broadleaf forests [36] [28]. Our workflow includes a normalised graph cut scheme to delineate ITCs using LiDAR 3D point cloud information alongside optical imagery [37].
- When selecting features to use in classification it is recognised that the dimensionality of hyperspectral data must be reduced to improve computationally efficiency, but hyperspectral imagery may have a significant noise component so we use robust PCA (rPCA) to prune data and strip away some of that noise [38].
- Finally, tree species classification at both pixel-level and ITC-level with support vector machine (SVM) [39] is implemented.

The main contribution of this paper is the development of a systematic workflow to map tree species at both pixel-level and ITC-level from multi-sensor imagery utilizing a combination of new and established approaches, which provide a powerful new approach for tree mapping. We test the efficiency of this approach by working with airborne imagery collected over a 18-ha mapped stand of temperate woodland in the UK. Historically managed temperate forests are recognised as being particularly difficult for ITC delineation because they have relatively even upper canopies comprised of intercalated crowns. To the best of our knowledge, only three studies have explored ITC-level species classification in a temperate forest [4], [29], [34].

The paper is organized as follows: in Section II, we introduce the temperate forest datasets tested in this paper. In Section III, we present our workflow for tree species classification at both pixel-level and ITC-level from LiDAR and hyperspectral sensors. The results and discussion are shown in Section IV. Conclusions and outlook are given in Section VI.

II. Data description

A. Study site and field data

Wytham Woods is a 385-ha deciduous forest, located in Oxfordshire, England (51°46′N, 1°20′W). A 18-ha forest plot was established in this wood in 2008 using standardised methods used in an international network of Smithsonian Institution Global Earth Observatories (SIGEO) [40]. Each hectare was delimited into 25 subplots of $20m \times 20m$. Every tree larger than 5cm diameter at chest height (DBH) was tagged, its DBH measured, its species identified and its location mapped. There were 23 species of tree and shrub within the plot. In total, 20,308 stems and 16,313 individual trees were recorded (some trees had multiple stems). These plots were re-censused in 2009 and 2012, and the latest dataset was used in this study.

As subcanopy species and shrubs are hard to detect by remote sensing, this study focuses on mapping the six most dominant canopy tree species listed in Table I. Tree height information is an important indicator for ITC-level species mapping. However, it was only measured on 389 individuals of these dominant canopy tree species. Species-specific functions were fitted to the height -diameters relationships ($H = a \ln DBH + b$, where a and b are coefficients estimated by linear regression) and these functions were used to estimate tree height information from DBH. We arbitrarily labeled trees >18m height as "canopy trees" (Table I) and used these to assess the accuracy of species detection. Figure 1 shows the linkage between field data, and training and testing samples taken from the airborne survey.

TABLE I
THE NUMBERS OF INDIVIDUAL AND CANOPY TREES OF SIX SPECIES RECORDED IN WYTHAM PLOT

Species	Common name	No. of individual trees	No. of canopy trees
Fraxinus excelsior	European ash	5346	1249
Acer pseudoplatanus	Sycamore	7716	778
Larix decidua	European larch	99	98
Quercus robur	English oak	381	201
Fagus sylvatica	European beech	195	4
Betula spp.	Birch	85	16

B. Airborne survey

Airborne surveying was conducted in the Wytham Woods natural reserve on 24 June 2014 by the Airborne Research and Survey Facility of the UK Natural Environment Research Council (NERC-ARSF). The airplane flew at a nominal height above ground of approximate 800 m and was equipped with LiDAR and hyperspectral imagers. LiDAR and hyperspectral imagery were pre-processed by NERC-ARSF Data Analysis Node.

Hyperspectral imagery was obtained by the AISA Fenix sensor, which is a pushbroom imaging array sensor with 384 cross-track pixels and provides 361 spectral bands from visible to shortwave infrared (0.4–2.5μm) region. The field of view of the AISA Fenix sensor is 31.94°. In this study, a single flight line of hyperspectral imagery was used, so illumination and sensor geometry was similar for all pixels. Atmospheric correction was not applied to the hyperspectral imagery. Although adjacency effects can influence the classification accuracy and atmospheric correction can reduce this problem, a number of studies have reported that applying an atmospheric correction has little effect on species classification [24], [33], [41], [42]. A bi-directional distribution function (BRDF) correction was not applied since a single flight line was used. If the hyperspectral imagery had

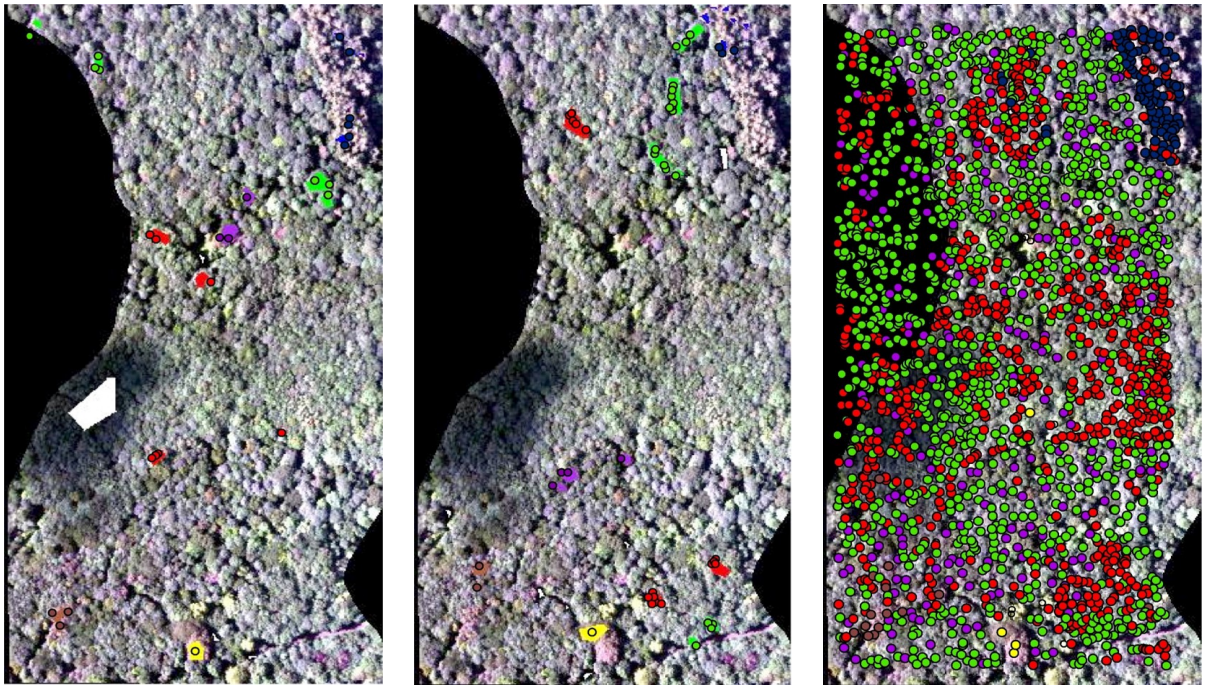

(a) Training samples (b) Test samples (c) Ground truth

Fig. 1. Training and testing samples for species classification in Wytham Woods. The coloured points in panel (a), (b) and (c) are ground truth overlaid over a false colour representation of the hyperspectral imagery. The coloured polygons in (a) and (b) represent training and testing samples of each species overlaid over a false colour representation of the hyperspectral imagery. Colours indicate different species, i.e., blue = *Larix decidua*, green = *Acer pseudoplatanus*, red = *Fraxinus excelsior*, yellow = *Fagus sylvatica*, purple = *Quercus robur*, brown = *Betula* spp., and white = shaded pixels.

been obtained from several flight lines, radiometric normalisation would have been needed in our workflow (Figure 2). The hyperspectral imagery was orthorectified and georeferenced in Ordinary Survey Great Britain (OSGB) projection, with spatial resolution of 1.2 m. The airborne LiDAR data were acquired by Leica ALS-50 II sensor. A scan angle of 12° was used. The LiDAR data were originally captured in full wave-form, however, they were converted to discrete LiDAR point cloud during the pre-processing step, within which the LiDAR point cloud was georeferenced in OSGB projection. The final point density was approximately 6 points/m^2. The equipment on board the NERC aircraft is regularly calibrated to ensure that LiDAR data are accurately georeferenced and the hyperspectral imagery is radiometrically calibrated before delivery.

III. Method

In this section, we present our processing workflow for pixel-level and ITC-level tree species classification from LiDAR and hyperspectral imagery, see Figure 2. The co-alignment step uses the NGF-Curv image registration method [35], the feature extraction from hyperspectral imagery is carried out with the rPCA method [38], the ITC delineation step uses a LiDAR point cloud based clustering method also informed by hyperspectral information, MCNCP-RNC [37], and, finally, the tree species classification at pixel-level and ITC-level is conducted with a SVM classifier [39] with the majority voting rule over each delineated crown area. The workflow in Figure 2 is very general, and the methods are described in greater detail below.

A. Co-alignment of LiDAR and hyperspectral imagery

Co-alignment of LiDAR and hyperspectral imagery can be achieved by ground control points or by unsupervised image registration. Our NGF-Curv method adopts the latter approach [35]. True colour composite of Red, Green and Blue (RGB) bands

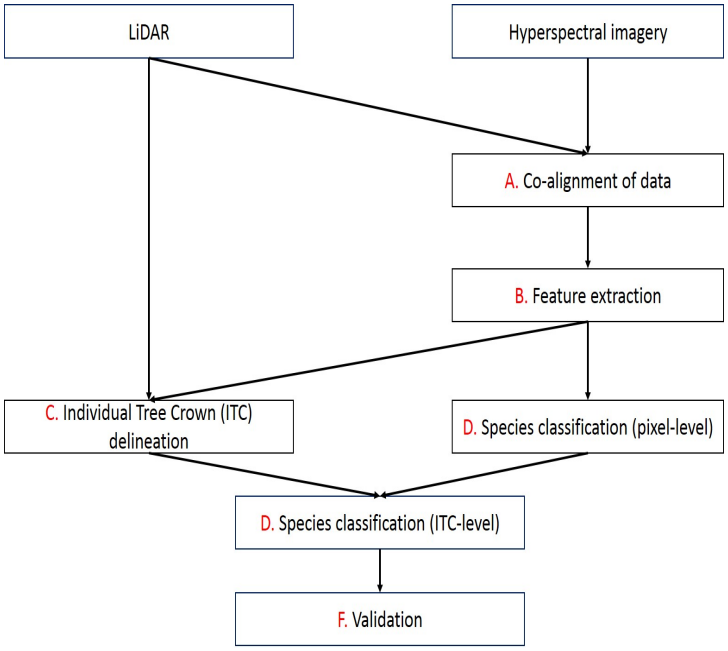

Fig. 2. Workflow used to detect individual tree crown and identify their species by fusing LiDAR and hyperspectral imagery.

(640, 549 and 460 nm) of hyperspectral imagery were converted to grey images by MATLAB build-in function `rgb2gray` and the grey image was used for registration purposes. LiDAR was converted to a digital surface model (DSM) by interpolating LiDAR first returns for the registration. Let reference (R) and template (T) images be the DSM taken from LiDAR and grey value image obtained from hyperspectral imagery, respectively. R and T are modeled as functions defined on a finite 2D grid Ω and mapping a point x on the grid to a real intensity value $R(x)$ and $T(x)$, respectively. The objective of the image registration is to find an optimal transformation mapping $u : \Omega \to \Omega$, in order to co-align the hyperspectral image onto the LiDAR raster image to obtain more accurate spatial resolution. The generic variational formulation of an image registration problem consists of a similarity term D and a regularisation term S minimising u:

$$\min_u \Big\{ \sum D[R(x), T(u(x))] + \alpha S(u) \Big\}$$

where α is the regularisation parameter which balances the similarity term and the regularisation term. The similarity term D used is defined by

$$1 - \left[\left(\frac{\nabla T(u)}{\sqrt{|\nabla T(u)|^2 + \eta^2}} \right)^T \left(\frac{\nabla R}{\sqrt{|\nabla R|^2 + \eta^2}} \right) \right]^2,$$

which is the so called NGF distance measure, where $\eta > 0$ is an edge parameter which represents the level of the noise in the images. To impose smoothness features on u, we use the curvature in the regularisation term S, i.e.

$$S(u) = \frac{1}{2} \sum_{x \in \Omega} |\Delta u(x)|^2.$$

For more details, we refer to [35] and references therein.

B. Feature extraction

Extracting feature information from the hyperspectral imagery is a key step to map individual trees with species information. As hyperspectral imagery contains a high number of spectral bands, i.e. dimensionality is high, the meaningful features are hidden inside an enormous number of spectral bands. To extract some or whole meaningful features, a data pruning technique rPCA [38] is implemented in our workflow.

Principal component analysis (PCA) finds a rank k matrix L from the $n \times m$ measurement matrix M, which may be corrupted by noise N. PCA can be expressed by following minimisation problem:

$$\min_{L}\{\|M - L\|_2\} \quad \text{s.t.} \quad \mathcal{R}(L) < k, \tag{1}$$

where $\|\cdot\|_2$ is ℓ_2-norm, and $\mathcal{R}(\cdot)$ is the operator computing the rank of the given matrix. Problem 1 is solved explicitly by singular value decomposition. However, the PCA is sensitive to the magnitude of noise in the data [43], thus it may not be suitable for extracting meaningful features from hyperspectral data. The rPCA method was proposed to improve the robustness of the PCA method [38]. Simply speaking, rPCA aim to recover a low rank matrix L from the corrupted measurement matrix M, which in our case is the hyperspectral imagery, by removing a sparse outlier matrix S. The rPCA method can be represented by the following minimization problem

$$\min_{L,S}\{\mathcal{R}(L) + \lambda\|S\|_0\} \quad \text{s.t.} \quad M = L + S, \tag{2}$$

where $\|\cdot\|_0$ is the ℓ_0-norm which counts the number of the nonzero entries therefore imposing sparsity property on S, λ is a regularisation parameter which balances the importance between the ranking operator and the sparsity regularisation. To make the above optimisation problem (2) tractable, its relaxation using the nuclear norm $\|\cdot\|_*$ (sum of singular values) and the l_1-norm (sum of the absolute values of the whole entries) were adopted instead of $\mathcal{R}(\cdot)$ and the l_0-norm respectively. This results in the following convex problem

$$\min_{L,S}\{\|L\|_* + \lambda\|S\|_1\} \quad \text{s.t.} \quad M = L + S. \tag{3}$$

More details about rPCA can be found in [38] and references therein. Since (3) is a convex problem, it can be solved effectively by, for example, the alternating direction method for multipliers (ADMM) [44]. In fact, the parameter λ is fixed to $\frac{1}{\sqrt{n}}$, where n is the number of rows of the measurement matrix M. The validity of the parameter choice of λ is given by [38, Theorem 1]. rPCA reduces the dimensionality of the hyperspectral imagery. In addition, a user can prune the data further. The validity of rPCA will be discussed in section V.

C. Individual tree crown delineation

Individual tree crown delineation is performed by a normalised graphcut method constrained by prior knowledge directly on the 3D LiDAR point clouds and the extracted features from subsection III-B. See [45] and method MCNCP-RNC [37] for the detailed methodology of the algorithm.

Let $\boldsymbol{G}$ be a graph containing a set of pairs, $\boldsymbol{G} = (\boldsymbol{\nu}, \boldsymbol{\epsilon})$, where $\boldsymbol{\nu}$ is the set of vertices and $\boldsymbol{\epsilon}$ is the set of edges. Each edge $w(\nu_i, \nu_j) \in \boldsymbol{\epsilon}$ is corresponding to the non-negative similarity weight $w_{i,j}$ between two vertices ν_i and ν_j. Such a graph is built on the LiDAR point clouds. The similarity weights depend on Euclidean distances between the LiDAR points and their intensity values as well as extracted features from hyperspectral imagery. The details of defining the weights, we refer to [37].

Let $\boldsymbol{W}$ be an $N \times N$ symmetric matrix with $\boldsymbol{W}(i,j) = w_{ij}$, $\boldsymbol{D}$ be an $N \times N$ diagonal matrix with diagonal entries $d_i = \sum_j w_{ij}$, $\mathbf{1}$ be an $N \times 1$ all-ones vector, $\boldsymbol{I}$ be a $C \times C$ identity matrix and $\boldsymbol{X}$ be an $N \times C$ matrix, where C is the number of clusters. The normalised cut is defined as

$$\begin{aligned} &\min_{\boldsymbol{X}} \operatorname{tr}\big(\boldsymbol{X}^T \boldsymbol{D}^{-\frac{1}{2}} (\boldsymbol{D} - \boldsymbol{W}) \boldsymbol{D}^{-\frac{1}{2}} \boldsymbol{X}\big) \\ &\text{s.t.} \quad \boldsymbol{X}^T \boldsymbol{D}^{\frac{1}{2}} \mathbf{1} = \mathbf{0}, \quad \boldsymbol{X}^T \boldsymbol{X} = \boldsymbol{I}, \end{aligned}$$

where $\operatorname{tr}(\cdot)$ is the trace of a matrix.

It is not straightforward to incorporate prior knowledge in normalised graphcut, as the normalised cut finds optimal partitioning from the graph of the similarity weights. In our modified scheme prior information is regarded as an additional constraint in the normalised graphcut approach. It minimises the normalised cut energy as well as satisfying a correlation constraint with priors. The correlation term $\operatorname{diag}(\boldsymbol{X}^T \boldsymbol{S}) = \kappa \operatorname{diag}(\boldsymbol{I})$ incorporates a prior information matrix S, which consists of the local maxima of the canopy height model (CHM) and their neighbour points. κ is a correlation coefficient. The CHM was obtained by normalising DSM with topography. The new modified normalised graphcut can be written as:

$$\begin{aligned} &\min_{\boldsymbol{X}} \operatorname{tr}\big(\boldsymbol{X}^T (\boldsymbol{D} - \boldsymbol{W}) \boldsymbol{X}\big) \\ &\text{s.t.} \quad \operatorname{diag}(\boldsymbol{X}^T \boldsymbol{X}) = \operatorname{diag}(\boldsymbol{I}), \quad \boldsymbol{X}^T \boldsymbol{D}^{\frac{1}{2}} \mathbf{1} = \mathbf{0}, \\ &\qquad \operatorname{diag}(\boldsymbol{X}^T \boldsymbol{S}) = \kappa \operatorname{diag}(\boldsymbol{I}). \end{aligned}$$

The locations of local maxima were computed by the toolbox for LiDAR data filtering and a standard forest analysis (TIFFS, Globalidar ltd.) [28]. Although we used TIFFS for extracting priors, users could use any tree top searching algorithm to get priors. We refer to [37] for more details.

D. Species classification

For the classification of the tree species we used the SVM method that is a non-parametric supervised classifier that has been showed to be superior to other classification strategies in several studies [22], [24], [33], [46]. We applied SVM on the extracted features from subsection III-B in order to classify species, initially at the pixel level.

For a training data set $\mathcal{T} = \{(x_1, y_1), \cdots, (x_n, y_n)\}$ consisting of pairs of feature vectors $x_i \in \mathcal{F}$ (where $\mathcal{F} \subset \mathbb{R}^m$ is a m-dimensional feature space), and labels y_i (for example the binary label $y_i \in \{-1, 1\}$). SVM finds a separating hyperplane $H := \{x \mid \langle w, \eta(x_i) \rangle - b) = 0\}$ (where w is a normal vector to the hyperplane, b is the intercept and $\eta(x_i) : \mathcal{F} \to \bar{\mathcal{F}}$ is a non-linear embedding that transforms the original feature space to a higher dimensional space). In this study, we adopt the radial basis (RBF) kernel $\exp(-\gamma \|x - x'\|_2^2)$ for η, where γ is the parameter for the radial basis.

!h

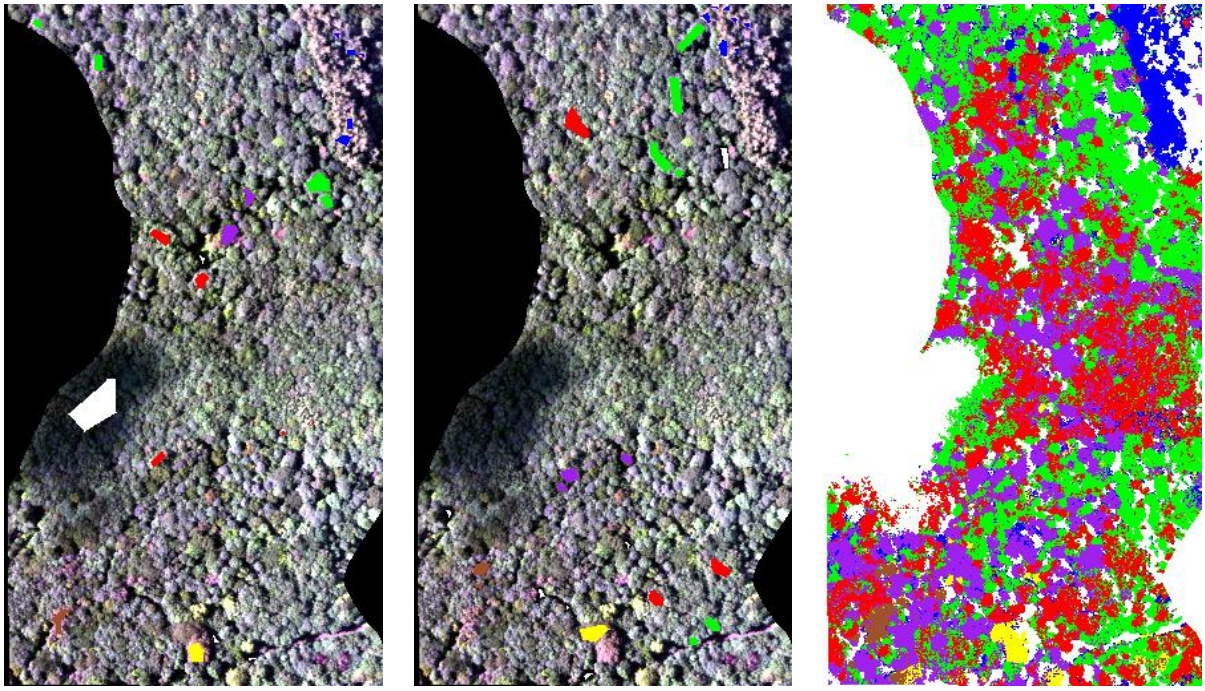

(a) Training samples (b) Test samples (c) Species classification map

Fig. 3. The pixel-level species classification in Wytham Woods. The coloured polygons in (a) and (b) represent training and test samples of each species overlaid over a false colour representation of the hyperspectral imagery. The colour map (c) shows the result of the pixel-level species classification by our proposed workflow. Colours indicate different species, i.e., blue = *Larix decidua*, green = *Acer pseudoplatanus*, red = *Fraxinus excelsior*, yellow = *Fagus sylvatica*, purple = *Quercus robur*, brown = *Betula* spp., and white = shaded pixels

The hyperplane H is then obtained by minimising the following model

$$\begin{aligned} &\min_{w,b,\xi} \|w\|_2^2 + C\sum_{i=1}^{n}\xi_i \\ &\text{s.t.} \quad y_i \cdot (\langle w, \eta(x_i)\rangle - b) \geq 1 - \xi_i \\ &\qquad \xi_i \geq 0 \end{aligned}$$

where C is a regularisation parameter and $\xi_i = \max(0, 1 - y_i \cdot \langle w, \eta(x_i)\rangle - b)$ is called a slack variable, which takes into account non-separable data.

SVM is an intrinsically binary classifier, but it can be extended to multi-class problems by following two different strategies: one-against-one and one-against-all. In this study, we use the one-against-all rule, which solves K binary problems instead of solving a K-class problem. We refer to [39] and references therein for an excellent introduction to SVM. A Library for SVM (libSVM) for MATLAB was used to solve the multi-class SVM problem [39]. The optimal parameters for SVM classification were found by trial and error. The regularisation parameter C was fixed to 100, and the parameter γ was set to 0.5 for all experiments in Section IV.

Figure 3 (a) and (b) show the location of the training and test samples used for the pixel-level tree species classification evaluation. Table II shows the number of pixels for each species used as training and test samples. The training and test samples of the hyperspectral imagery were extracted from manually delineated ITC by means of visual inspection and field

TABLE II
NUMBER OF PIXELS FOR EACH SPECIES OF THE TRAINING AND TEST SAMPLES FOR TREE SPECIES CLASSIFICATION

Species	Training samples	Test samples
Fraxinus excelsior	284	458
Acer pseudoplatanus	350	647
Larix decidua	144	135
Quercus robur	228	188
Fagus sylvatica	133	192
Betula spp.	106	105
Shade	824	109
Overall (NO. of pixels)	2069	1834

data. We considered only trees with height above 18m. It makes sense to mask out understory trees since spectral signatures captured from the hyperspectral imagery mainly originate from canopy leaves. The ITC-level tree species classification map is obtained by extracting the pixel level map for each ITC and applying a majority voting rule [9], [33] to decide the species for each crown (ITC-level). Therefore, the most frequent species class inside of each ITC represents the species of ITCs.

IV. RESULTS

This section presents the experimental results of our individual tree species classification workflow. We present the results of using both PCA and rPCA in the feature extraction step of the workflow to explore whether rPCA delivers more accurate results. We refer to workflows using PCA and rPCA in the feature extraction step ITSC method and ITSC-R method, respectively. For the results shown here, the feature extraction was applied only to the hyperspectral imagery.

Figure 4 shows the results of steps A, B and C of the workflow of Figure 2: Figure 4 (a) and (b) show the LiDAR (CHM) and a false colour representation of the hyperspectral imagery, and Figure 4 (c) shows the co-alignment result using the NGF-Curv registration method [35]. Since the initial alignment between LiDAR and hyperspectral imagery was excellent, any errors were too small to be apparent visually in our dataset. Figure 4 (d)–(g) show the first three principal components obtained by the rPCA method and their RGB colour composite. In our workflow, the first 20 principal components were used to delineate ITCs along with LiDAR using the MCNCP-RNC, and classify species in pixel and ITC levels. Figure 4 (h)–(j) show the ITC delineation results using the ITC delineation method MCNCP-RNC proposed in [37]. The tree species classification was evaluated at both pixel- and ITC-level. Producer's, user's and overall accuracies were computed starting from the confusion matrix. In addition, cohen's kappa, quantity and allocation disagreement were computed for the reliability of the classification results (see Table III, IV and V) [47].

A. Pixel-level tree species classification

Figure 3 (c) shows the species classification results over the 18-ha field plot in Wytham Woods. The results over the test samples were presented in Tables III and IV. The overall accuracy of the ITSC-R method at pixel-level was 89.1% while that of the ITSC method was 84.8%. In overall, the ITSC-R method showed better performances compared to the ITSC method. More details are given in the following.

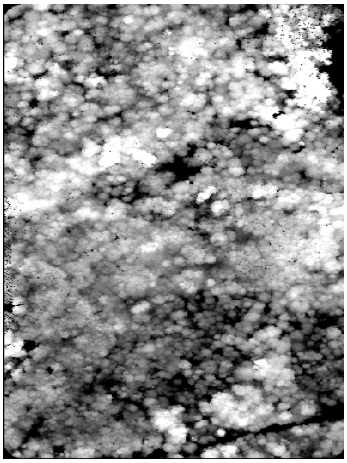

(a) LiDAR

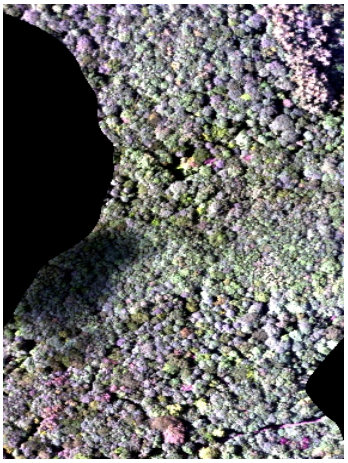

(b) Hyperspectral imagery

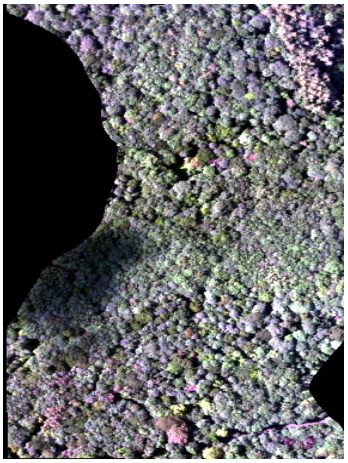

(c) Co-aligned hyperspectral imagery

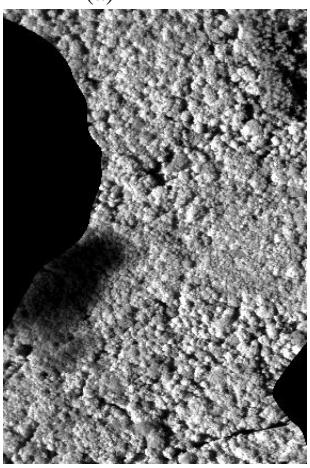

(d) 1^{st} principal component

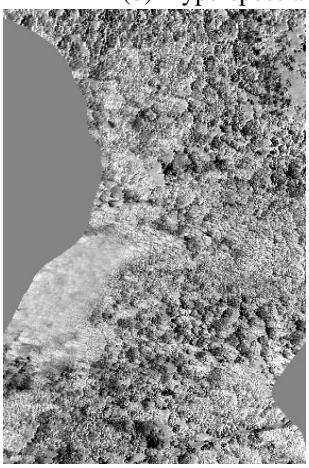

(e) 2^{ed} principal component

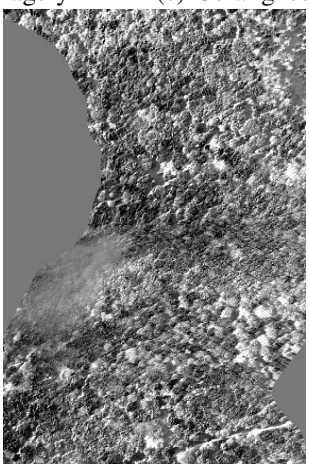

(f) 3^{rd} principal component

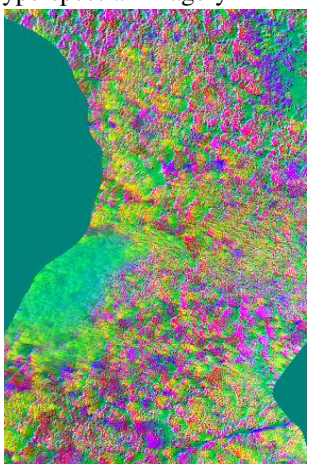

(g) Colour composite of the first 3 principal components

(h) ITCs of *Fraxinus excelsior*

(i) ITCs of *Acer pseudoplatanus*

(j) ITCs of *Quercus robur*

Fig. 4. The results of the images co-alignment, feature reduction and ITC delineation in our workflow. The first row shows the image registration between LiDAR DSM (a) and RGB true colour hyperspectral imagery (b) and the co-aligned hyperspectral imagery in RGB true colour (c). The second row shows the first three principal components (d)-(g). The third row shows examples of the MCNCP-RNC segmentation viewed obliquely (h)-(j) and different colours represent ITCs.

Regarding the individual species, for *Fraxinus excelsior* , the producer's accuracy was 82.3% and 87.5% for the ITSC-R and ITSC methods, respectively, but the ITSC-R method performed better with respect to the user's accuracy. The ITSC-R method outperformed the ITSC method for producer's accuracy and user's accuracy of *Acer pseudoplatanus*. The ITSC-R

TABLE III
SPECIES CLASSIFICATION RESULTS FROM THE ITSC METHOD

		Ground truth								
	Species	*Fraxinus excelsior*	*Acer pseudoplatanus*	*Larix decidua*	*Quercus robur*	*Fagus sylvatica*	*Betula* spp.	Shade	Total	Producer's accuracy (%)
Classification results	*Fraxinus excelsior*	401	35	0	21	0	0	1	458	87.5
	Acer pseudoplatanus	60	543	4	38	0	2	0	647	83.9
	Larix decidua	0	2	132	0	0	1	0	135	97.7
	Quercus robur	0	0	7	181	0	0	0	188	96.2
	Fagus sylvatica	0	17	41	6	114	11	3	192	59.3
	Betula spp.	2	2	6	15	2	76	2	105	72.3
	Shade	0	0	0	1	0	0	108	109	99.0
	Total	463	599	190	262	116	90	114	1834	
	User's accuracy (%)	86.6	88.2	69.4	69.0	98.3	85.7	94.7		84.8

Kappa accuracy = 0.807, Quantity disagreement = 0.076, Allocation disagreement= 0.076

TABLE IV
SPECIES CLASSIFICATION RESULTS OBTAINED BY THE ITSC-R METHOD

		Ground truth								
	Species	*Fraxinus excelsior*	*Acer pseudoplatanus*	*Larix decidua*	*Quercus robur*	*Fagus sylvatica*	*Betula* spp.	Shade	Total	Producer's accuracy (%)
Classification results	*Fraxinus excelsior*	378	31	3	44	0	0	2	458	82.3
	Acer pseudoplatanus	30	573	2	41	0	0	1	647	88.6
	Larix decidua	0	0	135	0	0	0	0	135	100
	Quercus robur	0	0	0	188	0	0	0	188	100
	Fagus sylvatica	0	0	9	7	168	2	6	192	87.5
	Betula spp.	0	1	2	3	14	84	1	105	80.0
	Shade	0	0	1	0	0	0	108	109	99.0
	Total	408	605	152	283	182	86	118	1834	
	User's accuracy (%)	92.7	94.7	88.8	66.9	92.3	97.7	91.5		89.1

Kappa accuracy = 0.861, Quantity disagreement = 0.066, Allocation disagreement= 0.043

method showed better performance with respect to producer's, while user's accuracies of *Quercus robur* were poor for both ITSC-R and ITSC methods. The confusion matrices of both ITSC-R and ITSC methods (Tables IV and III) show that *Fraxinus excelsior* was confused mainly with *Acer pseudoplatanus* and *Quercus robur*. *Acer pseudoplatanus* was confused with *Fraxinus excelsior* and *Quercus robur*. *Quercus robur* was a major confusing factor of both *Fraxinus excelsior* and *Acer pseudoplatanus*. Indeed this is the reason of the low user's accuracy of *Quercus robur*. It makes sense as the ground truth data in Figure 5 clearly shows that these three species are dominant in the study site and often are mixed.

Larix decidua was dominant at the north east edge of the study site, and both ITSC-R method and ITSC method successfully classified all the test samples of *Larix decidua*. However, *Larix decidua* was the major confusing factor for *Fagus sylvatica* pixels, so the user's accuracy of *Larix decidua* was poor for the ITSC method. The producer's accuracy of *Fagus sylvatica* was only 59.3% for the ITSC method as it was confused with *Larix decidua* pixels. For the ITSC-R method, the producer's and user's accuracies were 87.5% and 92.3%, respectively. The producer's accuracy of *Betula* species were only 72.3% for the ITSC method, while the ITSC-R method achieved 80.0% producer's accuracy. With respect to the user's accuracy of *Betula* species, the ITSC-R method achieved 97.5%, while the ITSC method only had 85.7%.

B. ITC-level species classification - mapping individual trees

Species classification at ITC-level was validated using a validation software for tree segmentation [48], [49]. This software uses tree heights and tree locations to find the best matching candidates between the ground truth and the segmented tree

crowns. The software, therefore, is still sensitive to the initial positioning of the ground truth. To alleviate this problem, we also included two figures to evaluate species classification at ITC-level. Figure 5 shows the both pixel- and ITC-level species classification results along with the ground truth information. Figure 6 shows the map of ITCs of each species using MCNCP-RNC method and the ground truth data. These two figures will be used to compare the patterns of species distribution across the study site.

In total, 1661 ITCs were delineated by MCNCP-RNC algorithm. However, the NEWFOR algorithm used to test delineation accuracy indicated that 677 ITCs were correctly delineated. The number of false positives generated by our algorithm were 960, while 964 ground truth trees were missing. The performance of ITC-level species classification was examined only for the 677 ITCs, which were corrected delineated by the validation software. However, the visual analysis of Figure 6 showed that the validation software does not accurately describe the performance of the ITC-level species classification. For example, *Larix decidua* is dominant at the north east edge of the study site. Since *Larix decidua* is a coniferous tree, it is relatively easy to delineate their crowns accurately. However, the validation results and table V show that almost 85% *Larix decidua* trees were omitted according to the validation results. In Figure 6(d) and (j), the patterns of *Larix decidua* from segmented ITCs and ground truth field data were very similar. This is mainly because the software is sensitive to the accuracy of tree coordinates in the ground data. Horizontal and vertical distances within 5 m between ground and segmented trees are considered to be matched. Since ground truth dataset had positioning errors of around 10 metres, large commission and omission errors arose.

Table V shows the confusion matrix at ITC-level, which considers only correctly assigned ITCs. The overall accuracy was only 65.8%, which was lower than that at pixel level. *Fraxinus excelsior* classification indicates that both producer's and user's accuracies were poor, while visual comparison of ground truth and species map in Figure 5 and Figure 6(a) and (g) show that species distribution patterns of ground truth and species map had a good agreement. The ITC-level classification of *Acer pseudoplatanus* was 72.7% and 77.1% with respect to producer's and user's accuracies. Visual inspection of Figure (b) and (h) suggested that ITC-level mapping of *Acer pseudoplatanus* agreed well with the ground truth data. *Larix decidua* was excluded from the validation as the ITC-level detection was unrealistic, but visual comparison implies that species distribution of pixel- and ITC-level were well agreed with the ground truth data. *Quercus robur* had a good producer's accuracy, while its user's accuracy was only 40.1%. This was in accordance with the pixel-level classification of *Quercus robur*. In particular, visual analysis of the ITC delineation suggests that *Quercus robur* was oversegmented (see Figure 6 (c) and (i). This might be because some branches were extracted as different local maxima, so the segmentation algorithm oversegmented the oak trees. The accuracy of *Fagus sylvatica* was similar with that of *Quercus robur*, so it had relatively high producer's accuracy and poor user's accuracy. Oversegmentation was observed in visual inspection, and indeed this was confirmed by the quantitative results: while there were only 4 trees in ground truths, twenty-five *Fagus sylvatica* were mapped by our workflow. This was partly because we only selected canopy trees over 18m, so some canopy trees were omitted. In addition, some branches of *Fagus sylvatica* were identified as local maxima, thereby causing commission errors. The accuracy of *Betula* spp. was the highest among all species in ITC-level classification. *Betula* spp. are located in a small area at southwest edge of the study site, so they can be mapped more easily (see Figure 6 (f) and (l)).

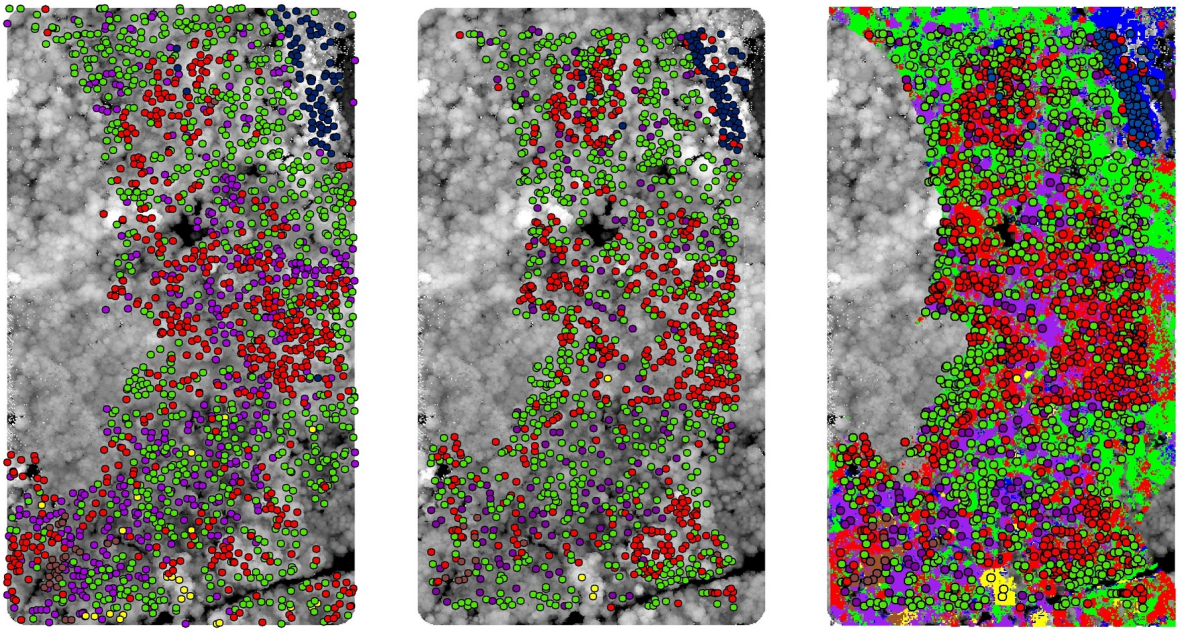

(a) ITC species mapping (b) Ground truth (c) Ground truth with pixel-level species classification

Fig. 5. Mapping individual tree species at ITC-level and ground truth. The background images in (a)-(c) are DSM. The coloured map in (c) is pixel-level species classification, where each colour indicates different species. The circles in colours represents ITCs of different species. blue = *Larix decidua*, green = *Acer pseudoplatanus*, red = *Fraxinus excelsior*, yellow = *Fagus sylvatica*, purple = *Quercus robur*, brown = *Betula* spp.

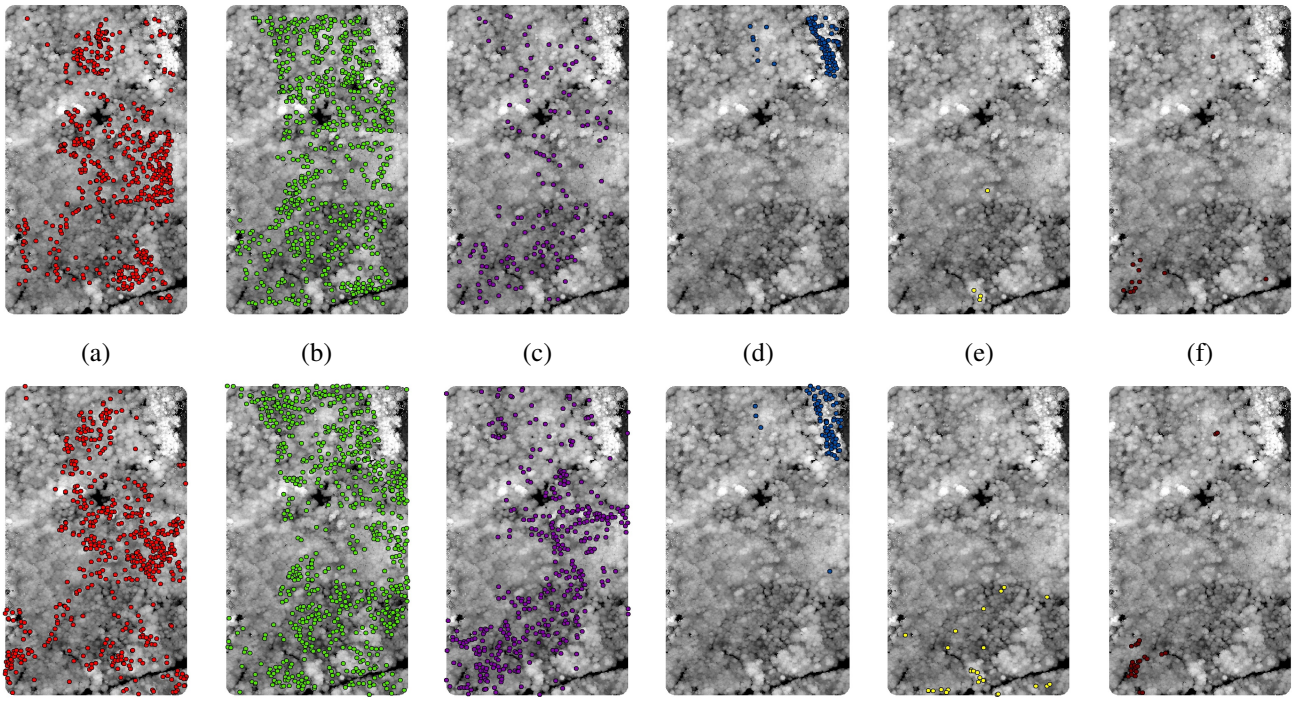

(a) (b) (c) (d) (e) (f)

(g) (h) (i) (j) (k) (l)

Fig. 6. Mapping each species at ITC-level and the ground truth. Each circle represents a single ITC. The first row shows the ground truths canopy trees over 18m. The second row shows the results of ITC-level species classification. Colours indicate different species, i.e., blue = *Larix decidua*, green = *Acer pseudoplatanus*, red = *Fraxinus excelsior*, yellow = *Fagus sylvatica*, purple = *Quercus robur*, brown = *Betula* spp.

TABLE V
SPECIES CLASSIFICATION RESULTS AT ITC-LEVEL.

		Ground truth								
	Species	*Fraxinus excelsior*	*Acer pseudoplatanus*	*Larix decidua*	*Quercus robur*	*Fagus sylvatica*	*Betula* spp.	Other species	Total	Producer's accuracy (%)
Classification results	*Fraxinus excelsior*	133	50	1	46	0	1	0	231	57.8
	Acer pseudoplatanus	53	243	2	35	1	0	0	334	72.7
	Larix decidua	3	4	5	1	0	0	0	13	38.4
	Quercus robur	2	11	0	55	4	0	0	72	76.3
	Fagus sylvatica	0	1	0	0	3	0	0	4	75.0
	Betula spp.	1	0	0	0	0	7	0	8	87.5
	Other species	5	6	4	0	0	0	0	15	0
	Total	197	315	12	137	8	8	0	677	-
	User's accuracy (%)	67.5	77.1	41.6	40.1	37.5	87.5	0	-	65.8

Kappa accuracy = 0.474, Quantity disagreement = 0.102, Allocation disagreement= 0.239

V. DISCUSSION

Feature reduction techniques provide rich information for distinguishing species with far fewer dimensions than the original hyperspectral datasets. Although spectral radiances of species the means of which are shown in Figure 5 (a) are significantly dependent on environmental conditions [50], there is a large degree of similarity among species. Figure 7 (a) shows that spectral radiance of *Fraxinus excelsior* and *Acer pseudoplatanus* are similar to each other and have greater radiance values than other species. The first principal components of PCA and rPCA reveal the same pattern, with *Fraxinus excelsior* and *Acer pseudoplatanus* having higher coefficients than the other species (Figure 7 (b) and (c)). It is important to note that PCA coefficients of different species tend to be similar for higher axes, so have little value in guiding species classification. In contrast, the coefficients from higher rPCA bands are very different among species, so provide meaningful signals with which to identify species

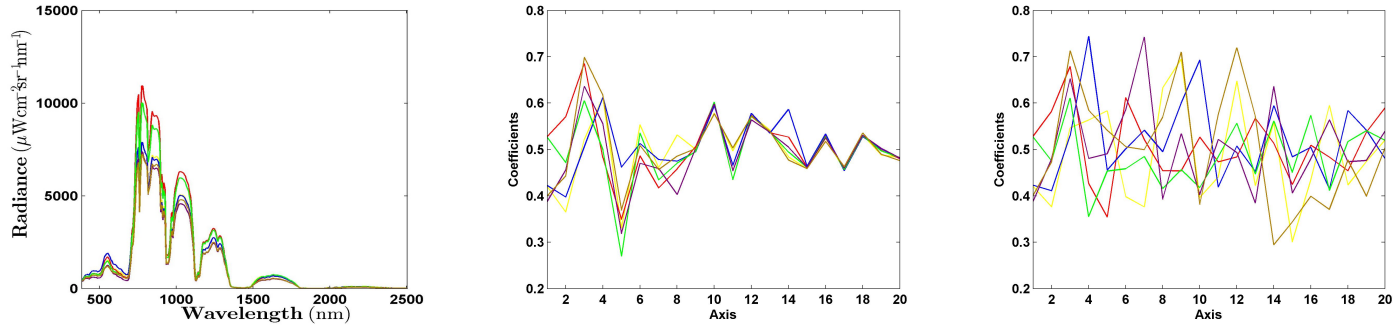

(a) Mean spectra (b) PCA coefficients (c) rPCA coefficients

Fig. 7. Spectral signatures of six dominant canopy tree species. Panel (a) shows spectral signatures of species, (b) and (c) are the mean coefficients of PCA and rPCA of species, respectively. Colours in (a)–(c) represent different species, i.e., blue = *Larix decidua*, green = *Acer pseudoplatanus*, red = *Fraxinus excelsior*, yellow = *Fagus sylvatica*, purple = *Quercus robur*, brown = *Betula* spp.

In this study, pixel-level species classification was conducted by only hyperspectral imagery because this study put more emphasis on improving species classification from hyperspectral imagery using rPCA technique. Many studies reported that using LiDAR features could improve species classification, since LiDAR is not influenced by illumination artefacts [22], [24]–[26]. LiDAR intensity may provide more detailed radiometric information for guiding species classification, however, in our acquisition LiDAR intensity was controlled in non-linear way by automatic gain control, thus it was not possible to calibrate

the intensity and to use it for species classification. In addition, illumination information is important for finding shaded pixels in our method, so the improvement by additional features from LiDAR may not be significant. Investigating the role of LiDAR derived metrics on species classification could provide better understanding of species classification, this is the beyond of the scope of this paper.

Species classification at pixel level is strongly influenced by illumination effects [14], [29], [33], [51]. Species classification using only sunlit pixels produce better results than considering all pixels (including shaded pixels) [14]. Thus a shadow removal step may be seen as a pre-requisite. Shadow removal can be done by manual selection [14], [27], ray tracing simulation with LiDAR derived DSM [51], ITC information from LiDAR [29] or normalised difference vegetation index filtering [32]. In this study, shaded pixels were included as additional class for learning (see Figure 3), such that shaded pixels were detected during the pixel-level species classification process as in Dalponte *et al.* [24]. This strategy is particularly useful as we can detect shaded pixels without particularly processing the shaded area. The producer's and user's accuracies of shaded pixel detection were high in both ITSC and ITSC-R methods. It is well-known that the first principal component is mainly related with illumination effects [52], which may be linked with high accuracy of shaded pixel detection of our method. Although Tochon *et al.* [52] report that the first component of PCA is not useful for ITC delineation, it can, at least, be used for more accurate pixel-level species classification by detecting shaded pixels.

The size of training dataset may affect the species classification result. In this paper Approximately 1–7 crowns per each species were used to classify all species and shaded pixels. Baldeck and Asner [53] showed that the sensitivity of species classification on sample size is dependent on the number of species and spectral separability of each species. In this study, the optimal number of tree crowns for species classification in a Savanna woodland was 10 trees for two species and 19 trees for eleven species; i.e. they used more tree samples. This difference might be related with the types of forest. We tested our workflow in a temperate forest, while their research was conducted in a Savanna woodland. We indeed used robust PCA to reduce 361 spectral bands to 20 principal components, therefore, direct comparison may not work. Moreover, airborne hyperspectral imagery used in this paper contained spectral signals spanning from the visible to SWIR (400–2500nm) wavelength region, on the other hand, the spectrometer used in [53] had spectral coverage from visible and NIR wavelength region (400–1000nm). The SWIR region may give more spectral separability, so it could reduce the sample size needed for species classification. Finding an optimal size of training samples in our test site requires further analysis, but we leave it for future work.

VI. Conclusion and outlook

This study investigated the possibility of species mapping using airborne remote sensing datasets. Although several algorithms have been suggested for species mapping over various types of forest, their system architectures assumed co-alignment of LiDAR and hyperspectral imagery, so it was difficult to apply directly. In addition, their methodologies for delineating ITC are mostly based on digital surface model rather than LiDAR point cloud, so both forest and ITC parameter estimation were relatively inaccurate. We introduced 3D tree delineation algorithm MCNCP-RNC in our proposed workflow, so forest analysis at species level, such as total biomass estimation of each canopy species, can be conducted more accurately. Our pixel-level species classification method showed that overall 89% of pixels were correctly assigned. However, the overall accuracy of ITC-level

tree species classification was only 65.8%. The low accuracy at the ITC-level classification might be related with inaccurate geopositioning of ground truth because visual analysis showed that species distribution patterns were well agreed with ground truth. In addition, errors might be related with illumination artefacts from hyperspectral imagery. Further research is required to evaluate our scheme with accurately georeferenced ground truth and improve ITC-level species delineation by correcting both illumination effects and overestimation of tree top priors.

VII. Acknowledgements

This project is supported by a grant from DEFRA / BBSRC to study the spread of ash dieback in British woodlands. The authors would like to thank NERC-ARSF for collecting and pre-processing the data used in this research project [RG13/08/175b], and a grant from the Isaac Newton Trust.

References

[1] G. Asner, D. Knapp, A. Balaji, and G. Páez-Acosta, "Automated mapping of tropical deforestation and forest degradation: Claslite," *Journal of Applied Remote Sensing*, vol. 3, no. 1, pp. 033 543–033 543, 2009.

[2] R. Houghton, K. Lawrence, J. Hackler, and S. Brown, "The spatial distribution of forest biomass in the brazilian amazon: a comparison of estimates," *Global Change Biology*, vol. 7, no. 7, pp. 731–746, 2001.

[3] Z. A. Latif, I. Zamri, and H. Omar, "Determination of tree species using worldview-2 data," in *Signal Processing and its Applications (CSPA), 2012 IEEE 8th International Colloquium on*. IEEE, 2012, pp. 383–387.

[4] M. Immitzer, C. Atzberger, and T. Koukal, "Tree species classification with random forest using very high spatial resolution 8-band worldview-2 satellite data," *Remote Sensing*, vol. 4, no. 9, pp. 2661–2693, 2012.

[5] K. Y. Peerbhay, O. Mutanga, and R. Ismail, "Investigating the capability of few strategically placed worldview-2 multispectral bands to discriminate forest species in kwazulu-natal, south africa," *Selected Topics in Applied Earth Observations and Remote Sensing, IEEE Journal of*, vol. 7, no. 1, pp. 307–316, 2014.

[6] G. Omer, O. Mutanga, E. M. Abdel-Rahman, and E. Adam, "Performance of support vector machines and artificial neural network for mapping endangered tree species using worldview-2 data in dukuduku forest, south africa," *Selected Topics in Applied Earth Observations and Remote Sensing, IEEE Journal of*, 2015.

[7] G. P. Asner, R. E. Martin, A. J. Ford, D. J. Metcalfe, and M. J. Liddell, "Leaf chemical and spectral diversity in australian tropical forests," *Ecological Applications*, vol. 19, no. 1, pp. 236–253, 2009.

[8] J.-B. Féret and G. P. Asner, "Spectroscopic classification of tropical forest species using radiative transfer modeling," *Remote Sensing of Environment*, vol. 115, no. 9, pp. 2415–2422, 2011.

[9] ——, "Tree species discrimination in tropical forests using airborne imaging spectroscopy," *Geoscience and Remote Sensing, IEEE Transactions on*, vol. 51, no. 1, pp. 73–84, 2013.

[10] G. P. Asner, "Biophysical and biochemical sources of variability in canopy reflectance," *Remote sensing of Environment*, vol. 64, no. 3, pp. 234–253, 1998.

[11] M. Cochrane, "Using vegetation reflectance variability for species level classification of hyperspectral data," *International Journal of Remote Sensing*, vol. 21, no. 10, pp. 2075–2087, 2000.

[12] K. L. Castro-Esau, G. A. Sánchez-Azofeifa, B. Rivard, S. J. Wright, and M. Quesada, "Variability in leaf optical properties of mesoamerican trees and the potential for species classification," *American Journal of Botany*, vol. 93, no. 4, pp. 517–530, 2006.

[13] G. Asner, J. Boardman, C. Field, D. Knapp, T. Kennedy-Bowdoin, M. Jones, and R. Martin, "Carnegie airborne observatory: in-flight fusion of hyperspectral imaging and waveform light detection and ranging for three-dimensional studies of ecosystems," *Journal of Applied Remote Sensing*, vol. 1, no. 1, pp. 013 536–013 536, 2007.

[14] M. L. Clark, D. A. Roberts, and D. B. Clark, "Hyperspectral discrimination of tropical rain forest tree species at leaf to crown scales," *Remote sensing of environment*, vol. 96, no. 3, pp. 375–398, 2005.

[15] J. Zhang, B. Rivard, A. Sánchez-Azofeifa, and K. Castro-Esau, "Intra-and inter-class spectral variability of tropical tree species at la selva, costa rica: Implications for species identification using hydice imagery," *Remote Sensing of Environment*, vol. 105, no. 2, pp. 129–141, 2006.

[16] M. A. Cho, P. Debba, R. Mathieu, L. Naidoo, J. Van Aardt, and G. P. Asner, "Improving discrimination of savanna tree species through a multiple-endmember spectral angle mapper approach: Canopy-level analysis," *Geoscience and Remote Sensing, IEEE Transactions on*, vol. 48, no. 11, pp. 4133–4142, 2010.

[17] C. A. Baldeck and G. P. Asner, "Single-species detection with airborne imaging spectroscopy data: A comparison of support vector techniques," *Selected Topics in Applied Earth Observations and Remote Sensing, IEEE Journal of*, vol. 8, no. 6, pp. 2501–2512, 2015.

[18] M. Dalponte, L. Bruzzone, L. Vescovo, and D. Gianelle, "The role of spectral resolution and classifier complexity in the analysis of hyperspectral images of forest areas," *Remote Sensing of Environment*, vol. 113, no. 11, pp. 2345–2355, 2009.

[19] K. M. Dahlin, G. P. Asner, and C. B. Field, "Environmental and community controls on plant canopy chemistry in a mediterranean-type ecosystem," *Proceedings of the National Academy of Sciences*, vol. 110, no. 17, pp. 6895–6900, 2013.

[20] N. Goodwin, R. Turner, and R. Merton, "Classifying eucalyptus forests with high spatial and spectral resolution imagery: an investigation of individual species and vegetation communities," *Australian Journal of Botany*, vol. 53, no. 4, pp. 337–345, 2005.

[21] R. Hill, A. Wilson, M. George, and S. Hinsley, "Mapping tree species in temperate deciduous woodland using time-series multi-spectral data," *Applied Vegetation Science*, vol. 13, no. 1, pp. 86–99, 2010.

[22] M. Dalponte, H. O. Orka, T. Gobakken, D. Gianelle, and E. Næsset, "Tree species classification in boreal forests with hyperspectral data," *Geoscience and Remote Sensing, IEEE Transactions on*, vol. 51, no. 5, pp. 2632–2645, 2013.

[23] M. Colgan, C. B. adn J. Féret, and G. Asner, "Mapping savanna tree species at ecosystem scales using support vector machine classification and brdf correction on airborne hyperspectral and lidar data," *Remote Sensing*, vol. 4, no. 11, pp. 3462–3480, 2012.

[24] M. Dalponte, L. Bruzzone, and D. Gianelle, "Fusion of hyperspectral and lidar remote sensing data for classification of complex forest areas," *Geoscience and Remote Sensing, IEEE Transactions on*, vol. 46, no. 5, pp. 1416–1427, 2008.

[25] T. G. Jones, N. C. Coops, and T. Sharma, "Assessing the utility of airborne hyperspectral and lidar data for species distribution mapping in the coastal pacific northwest, canada," *Remote Sensing of Environment*, vol. 114, no. 12, pp. 2841–2852, 2010.

[26] M. Dalponte, L. Bruzzone, and D. Gianelle, "Tree species classification in the southern alps based on the fusion of very high geometrical resolution multispectral/hyperspectral images and lidar data," *Remote sensing of environment*, vol. 123, pp. 258–270, 2012.

[27] A. Ghosh, F. E. Fassnacht, P. Joshi, and B. Koch, "A framework for mapping tree species combining hyperspectral and lidar data: Role of selected classifiers and sensor across three spatial scales," *International Journal of Applied Earth Observation and Geoinformation*, vol. 26, pp. 49–63, 2014.

[28] Q. Chen, D. Baldocchi, P. Gong, and M. Kelly, "Isolating individual trees in a savanna woodland using small footprint lidar data," *Photogrammetric Engineering and Remote Sensing*, vol. 72, no. 8, pp. 923–932, 2006.

[29] J. Heinzel and B. Koch, "Investigating multiple data sources for tree species classification in temperate forest and use for single tree delineation," *International Journal of Applied Earth Observation and Geoinformation*, vol. 18, pp. 101–110, 2012.

[30] C. Zhang and F. Qiu, "Mapping individual tree species in an urban forest using airborne lidar data and hyperspectral imagery," *Photogrammetric Engineering & Remote Sensing*, vol. 78, no. 10, pp. 1079–1087, 2012.

[31] M. Voss and R. Sugumaran, "Seasonal effect on tree species classification in an urban environment using hyperspectral data, lidar, and an object-oriented approach," *Sensors*, vol. 8, no. 5, pp. 3020–3036, 2008.

[32] M. Alonzo, B. Bookhagen, and D. A. Roberts, "Urban tree species mapping using hyperspectral and lidar data fusion," *Remote Sensing of Environment*, vol. 148, pp. 70–83, 2014.

[33] M. Dalponte, H. O. Ørka, L. T. Ene, T. Gobakken, and E. Næsset, "Tree crown delineation and tree species classification in boreal forests using hyperspectral and als data," *Remote sensing of environment*, vol. 140, pp. 306–317, 2014.

[34] R. Dinuls, G. Erins, A. Lorencs, I. Mednieks, and J. Sinica-Sinavskis, "Tree species identification in mixed baltic forest using lidar and multispectral data," *Selected Topics in Applied Earth Observations and Remote Sensing, IEEE Journal of*, vol. 5, no. 2, pp. 594–603, 2012.

[35] J. Lee, X. Cai, C.-B. Schölieb, and D. Coomes, "Nonparametric image registration of airborne lidar, hyperspectral and photographic imagery of wooded landscapes," *Geoscience and Remote Sensing, IEEE Transactions on*, in press.

[36] A. Persson, J. Holmgren, and U. Söderman, "Detecting and measuring individual trees using an airborne laser scanner," *Photogrammetric Engineering and Remote Sensing*, vol. 68, no. 9, pp. 925–932, 2002.

[37] J. Lee, X. Cai, J. Lellmann, C.-B. Schönlieb, and D. Coomes, "3d individual tree segmentation from fully integrated lidar, hyperspectral imagery and aerial photographs," *Technical report, DAMTP, Cambridge*, 2015.

[38] E. J. Candès, X. Li, Y. Ma, and J. Wright, "Robust principal component analysis?" *Journal of the ACM (JACM)*, vol. 58, no. 3, p. 11, 2011.

[39] C.-C. Chang and C.-J. Lin, "LIBSVM: A library for support vector machines," *ACM Transactions on Intelligent Systems and Technology*, vol. 2, pp. 27:1–27:27, 2011, software available at http://www.csie.ntu.edu.tw/~cjlin/libsvm.

[40] N. Butt, G. Campbell, Y. Malhi, M. Morecroft, K. Fenn, and M. Thomas, "Initial results from establishment of a long-term broadleaf monitoring plot at wytham woods, oxford, uk," *University of Oxford Report*, 2009. [Online]. Available: http://ctfs.si.edu/Public/plotdataaccess/TermsConditions.php?plotid=30&typedata=tree

[41] J. P. Hoffbeck, D. Landgrebe *et al.*, "Effect of radiance-to-reflectance transformation and atmosphere removal on maximum likelihood classification accuracy of high-dimensional remote sensing data," in *Geoscience and Remote Sensing Symposium, 1994. IGARSS'94. Surface and Atmospheric Remote Sensing: Technologies, Data Analysis and Interpretation., International*, vol. 4. IEEE, 1994, pp. 2538–2540.

[42] H.-R. Y. Sun-Hwa Kim, Jung-Il Shin and K.-S. Lee, "Effect of atmospheric correction for the land cover classification using hyperspectral data," *Proceeding of 2006 Asian Conference on Remote Sensing*, 2006.

[43] I. Jolliffe, *Principal component analysis*. Wiley Online Library, 2002.

[44] X. Yuan and J. Yang, "Sparse and low-rank matrix decomposition via alternating direction methods," *preprint*, 2009.

[45] H. Hu, J. Feng, C. Yu, and J. Zhou, "Multi-class constrained normalized cut with hard, soft, unary and pairwise priors and its applications to object segmentation," *Image Processing, IEEE Transactions on*, vol. 22, no. 11, pp. 4328–4340, 2013.

[46] J.-B. Féret and G. P. Asner, "Semi-supervised methods to identify individual crowns of lowland tropical canopy species using imaging spectroscopy and lidar," *Remote Sensing*, vol. 4, no. 8, pp. 2457–2476, 2012.

[47] R. G. Pontius Jr and M. Millones, "Death to kappa: birth of quantity disagreement and allocation disagreement for accuracy assessment," *International Journal of Remote Sensing*, vol. 32, no. 15, pp. 4407–4429, 2011.

[48] NEWFOR, "Alpine space programme, european territorial cooperation 2007-2013-project newfor," 2012. [Online]. Available: http://www.newfor.net/projet/

[49] L. Eysn, M. Hollaus, E. Lindberg, F. Berger, J.-M. Monnet, M. Dalponte, M. Kobal, M. Pellegrini, E. Lingua, D. Mongus *et al.*, "A benchmark of lidar-based single tree detection methods using heterogeneous forest data from the alpine space," *Forests*, vol. 6, no. 5, pp. 1721–1747, 2015.

[50] R. Richter and D. Schläpfer, "Atmospheric/topographic correction for airborne imagery," *ATCOR-4 user guide*, 2011.

[51] E. Puttonen, P. Litkey, and J. Hyyppä, "Individual tree species classification by illuminated–shaded area separation," *Remote Sensing*, vol. 2, no. 1, pp. 19–35, 2009.

[52] G. Tochon, J. Féret, S. Valero, R. Martin, D. Knapp, P. Salembier, J. Chanussot, and G. Asner, "On the use of binary partition trees for the tree crown segmentation of tropical rainforest hyperspectral images," *Remote Sensing of Environment*, vol. 159, pp. 318–331, 2015.

[53] C. A. Baldeck and G. P. Asner, "Improving remote species identification through efficient training data collection," *Remote Sensing*, vol. 6, no. 4, pp. 2682–2698, 2014.